Development of ^{111}In-Labeled Liposomes for Vulnerable Atherosclerotic Plaque Imaging

Mikako Ogawa[1], Izumi O. Umeda[2], Mutsumi Kosugi[1], Ayumi Kawai[1], Yuka Hamaya[1], Misato Takashima[1], Hongxia Yin[3], Takayuki Kudoh[3], Masaharu Seno[3], and Yasuhiro Magata[1]

[1]Medical Photonics Research Center, Hamamatsu University School of Medicine, Hamamatsu, Japan; [2]National Cancer Center Hospital East, Chiba, Japan; and [3]Graduate School of Natural Science and Technology, Okayama University, Okayama, Japan

Macrophage infiltration is a common characteristic feature of atherosclerotic-vulnerable plaques. Macrophages recognize phosphatidylserine (PS) exposed on the surface of apoptotic cells, which triggers the engulfment of the apoptotic cells by macrophages through phagocytosis. In this study, we prepared radiolabeled PS liposomes for detection of vulnerable plaques. **Methods:** PS liposomes were prepared by lipid film hydration. Phosphatidylcholine (PC) liposomes were prepared as controls. Liposomes (100 or 200 nm) were generated by an extruder to produce PS100, PS200, PC100, and PC200 liposomes. These were then radiolabeled by encapsulating ^{111}In-nitrilotriacetic acid using an active-loading method. ^{111}In liposomes were incubated with cultured macrophages for 2 h, and the uptake level was measured. For biodistribution studies, the ^{111}In liposomes were injected intravenously into ddY mice. In addition, the ^{111}In liposomes were injected into apolipoprotein E–deficient (apoE−/−) mice, and the aortas were harvested for autoradiography and oil red O staining. For SPECT imaging, ^{111}In liposomes were injected intravenously into Watanabe heritable hyperlipidemic rabbits and scanned 48 h after injection. **Results:** The radiochemical yields were greater than 95% for all the prepared ^{111}In liposomes. The level of in vitro uptake by macrophages was 60.5, 14.7, 32.0, and 14.4 percentage injected dose per milligram of protein for ^{111}In-PS100, ^{111}In-PC100, ^{111}In-PS200, and ^{111}In-PC200, respectively. In biodistribution studies, high spleen uptake was seen with PC liposomes. Liver uptake was high for all liposomes but was lowest with ^{111}In-PS200. The blood half-lives were 3.2, 22.0, 3.6, and 7.4 min for ^{111}In-PS100, ^{111}In-PC100, ^{111}In-PS200, and ^{111}In-PC200, respectively. The distribution of ^{111}In-labeled PS liposomes into atherosclerotic regions determined by autoradiography was well matched with the results of oil red O staining in apoE−/− mice. The target-to-nontarget ratios were 2.62, 2.23, 3.27, and 2.51 for ^{111}In-PS100, ^{111}In-PC100, ^{111}In-PS200, and ^{111}In-PC200, respectively. The aorta was successfully visualized by SPECT at 48 h after ^{111}In-labeled PS liposome injection; however, high liver uptake was also observed. **Discussion:** From the in vitro uptake study, it has been demonstrated that macrophage targeting was accomplished by PS modification. Also, an atherosclerotic region was successfully detected by ^{111}In-PS200 in apoE−/− mice and Watanabe heritable hyperlipidemic rabbits in vivo. Liposome modification to obtain slower blood clearance and lower liver uptake would be required to improve the SPECT images.

Key Words: atherosclerosis; phosphatidylserine; liposome; SPECT

J Nucl Med 2014; 55:115–120
DOI: 10.2967/jnumed.113.123158

Vulnerable plaques in atherosclerotic lesions can cause acute myocardial infarction and stroke. Therefore, detection of high-risk, vulnerable plaque is important for risk stratification and to facilitate early treatment. Macrophage infiltration is a characteristic of vulnerable plaques, and macrophages play a central role in the destabilization of atherosclerotic lesions (*1,2*). We and other groups have previously reported that because macrophages are metabolically active, vulnerable plaques can be detected with the glucose analog ^{18}F-FDG by PET (*3–6*). Thus, ^{18}F-FDG PET can be a useful tool for detecting vulnerable plaques, and the method has been used in both animal investigations and clinical studies (*7–10*). However, glucose consumption is not a specific phenomenon for macrophages, and glucose concentration affects ^{18}F-FDG accumulation in macrophages (*11,12*). Thus, blood sugar level needs to be well controlled for accurate evaluation of vulnerable plaques by ^{18}F-FDG. Because diabetes often coexists with atherosclerosis, this would create some difficulties in such patients. Furthermore, there would be some difficulties associated with coronary artery imaging, because of physiologic accumulation of ^{18}F-FDG in the heart.

In this study, we developed a liposome-based imaging probe that targets macrophages. Liposomes have been shown to be safe for human use, and they can be a suitable platform for multimodal imaging (*13–15*). In addition, it is well known that macrophages phagocytize particles such as liposomes (*16,17*). Furthermore, we applied surface modification to the liposomes for more effective macrophage targeting. In atherosclerotic-vulnerable plaques, many apoptotic cells are produced in a sequence of inflammatory reactions. In atherosclerotic regions, macrophages recognize phosphatidylserine (PS) on the surface of apoptotic cells, which triggers the macrophages to phagocytize the apoptotic cells (*18–21*). Therefore, in this study, we prepared PS-modified liposomes and radiolabeled them with ^{111}In for SPECT imaging. We first evaluated the effect of PS modification of the liposomes on macrophage uptake in vitro. After investigating the in vivo kinetics of the liposomes in normal mice, imaging studies were performed in apolipoprotein E–deficient (apoE−/−) mice for quantitative analysis, and in Watanabe heritable hyperlipidemic (WHHL) rabbits for SPECT imaging.

Received Mar. 14, 2013; revision accepted Sep. 3, 2013.
For correspondence or reprints contact: Mikako Ogawa, Department of Molecular Imaging, Medical Photonics Research Center, Hamamatsu University of School of Medicine, 1-20-1 Handayama, Higashiku, Hamamatsu 431-3192, Japan.
E-mail: mogawa@hama-med.ac.jp
Published online Dec. 12, 2013.

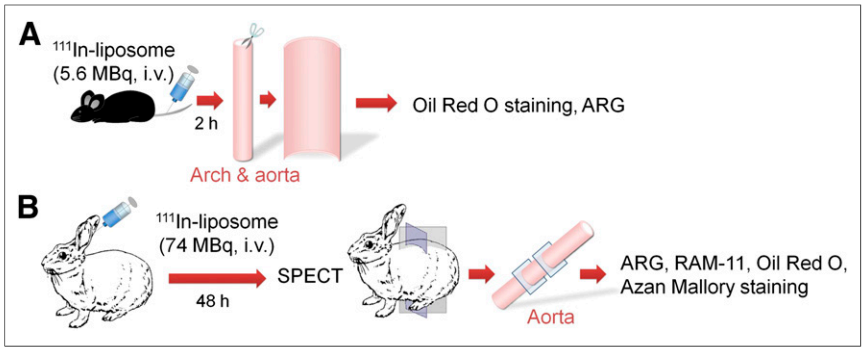

FIGURE 1. Timeline diagrams for animal studies. (A) Ex vivo autoradiography in apoE−/− mice. (B) SPECT imaging, ex vivo autoradiography, and histologic analysis in WHHL rabbits. ARG = autoradiography; i.v. = intravenously.

MATERIALS AND METHODS

Materials

Distearoylphosphatidylcholine and distearoylphosphatidyl-L-serine were purchased from NOF Corp. Diethylenetriaminepentaacetic acid and 8-hydroxyquinoline were purchased from Wako Pure Chemicals. ^{111}In-$InCl_3$ was obtained from Nihon Medi-Physics Co., Ltd. All other chemicals used were reagent grade. Male ddY mice were supplied by Japan SLC Co., Ltd. ApoE−/− mice were purchased from The Jackson Laboratory. WHHL rabbits and New Zealand White rabbits were purchased from Kitayama Labes Co., Ltd. The present animal study was approved by the Animal Care and Use Committee of the Hamamatsu University School of Medicine.

Synthesis of Dipalmitoylphosphatidyl D-Serine

Dipalmitoylphosphatidyl D-serine was synthesized according to the procedure of Lindh and Stawińsky (*22*). The details are described in the Supplemental Appendix (supplemental materials are available at http://jnm.snmjournals.org).

Preparation of Liposomes

PS-modified liposomes and control liposomes (phosphatidylcholine [PC] liposomes) were prepared. To investigate the specificity for PS, which incorporates the naturally occurring L-serine form, phosphatidyl-D-serine (D-PS)–containing liposomes (D-PS liposomes) were also prepared. Prepared sizes were 100 and 200 nm for each liposome type.

Liposomes were prepared by the lipid film hydration-extrusion method (*23*). The details are described in the Supplemental Appendix.

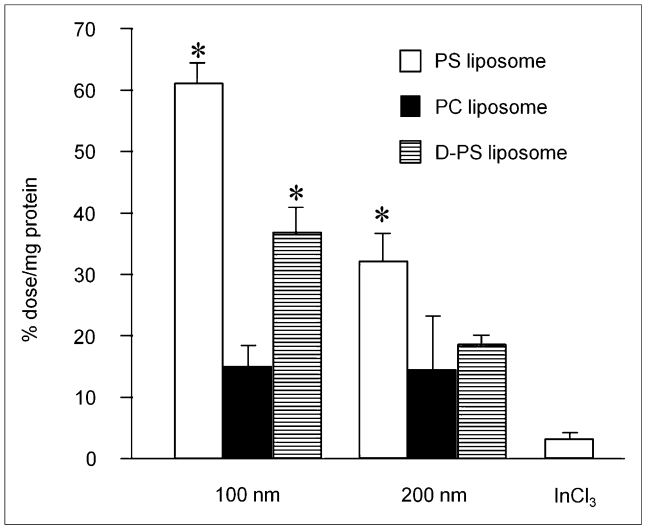

FIGURE 2. ^{111}In-labeled liposome uptake by cultured macrophages. Significantly higher uptake was observed in PS liposomes than PC liposomes of each size (*$P < 0.05$). D-isomer of PS liposomes showed lower uptake than L-isomers.

Radiolabeling of Liposomes

The liposomes were radiolabeled by the remote-loading method. Briefly, ^{111}In-$InCl_3$ solution was mixed with 51 mM oxine (8-quinolinol) in ethanol and incubated in 2 M sodium acetate buffer for 10 min at 40°C to prepare the loading solution. Nitrilotriacetic acid (NTA)–encapsulated liposomes were incubated in the loading solution for 10 min at 40°C for transchelation between NTA and oxine. The excess ^{111}In-oxine was removed by ultracentrifugation (37,500*g*, 30 min). The mechanism of radionuclide transport through the lipid bilayer can be summarized as follows. Oxine is a lipophilic chelating ligand that can be distributed to both the aqueous phase and the liposomal lipid membrane. Under the indicated experimental conditions, the oxine concentration is approximately 1,000- to 100,000-fold in excess of ^{111}In, meaning that practically all ^{111}In ions are coordinated to oxine at equilibrium. The resulting ^{111}In-oxine complex diffuses across the lipid bilayer from outside of the liposome to inside, followed by transchelation with NTA (a stronger chelator) inside the liposome aqueous core. Thus, ^{111}In-labeled PS liposomes (100 and 200 nm [^{111}In-PS100 and ^{111}In-PS200, respectively]), ^{111}In-labeled D-PS liposomes (100 and 200 nm [^{111}In-DPS100 and ^{111}In-DPS200, respectively]), and ^{111}In-labeled PC liposomes (100 and 200 nm [^{111}In-PC100 and ^{111}In-PC200, respectively]) were prepared.

Macrophage Isolation

Mouse peritoneal macrophages were isolated as previously described, with slight modifications (*24*). Four days after the 10% thioglycolate injection (intraperitoneal) into female ddY mice, the animals were sacrificed and macrophages were isolated from the peritoneal cavity by phosphate-buffered saline (PBS) lavage. Macrophages were plated into 6-well plates and cultured in Dulbecco modified Eagle medium (glucose, 4,000 mg/L; Sigma-Aldrich Co.) supplemented with 10% fetal bovine serum and penicillin and streptomycin (100 U/mL) at 37°C in 95% air–5% CO_2.

^{111}In-Labled Liposome Uptake by Cultured Macrophages

Plated macrophages were cultured for 24 h and washed with PBS. Macrophages were then preincubated with 2 mL of Dulbecco modified Eagle medium at 37°C for 1 h. Subsequently, 7.4 kBq of ^{111}In-PS100, ^{111}In-DPS100, ^{111}In-PC100, ^{111}In-PS200, ^{111}In-DPS200, or ^{111}In-PC200 liposomes were added to wells and incubated at 37°C for 2 h in 95% air–5% CO_2. In addition, for controls, ^{111}In-$InCl_3$ (7.4 kBq) was added to additional wells. After incubation, the medium was removed, and the cells were rinsed twice with 1 mL of PBS. The washings were combined with the removed medium. Macrophages were scraped from the wells in 0.35 mL of PBS, and the wells were rinsed with an additional 0.35 mL of PBS, which was combined with the cell suspension. The radioactivity of medium and cell suspension was measured with an automated γ counter (Wizard^2 3"; Perkin Elmer Inc.). After radioactivity measurement, the protein concentration was determined by the method of Lowry et al. (*25*). Uptake of ^{111}In-labeled liposomes was expressed as the ratio of radioactivity in the cell to the initial dose per milligram of protein.

Biodistribution Studies

Male ddY mice (6 wk) were injected with 37 kBq of ^{111}In-PS100, ^{111}In-PC100, ^{111}In-PS200, or ^{111}In-PC200 liposomes via the tail vein

TABLE 1
Biodistribution of ^{111}In-PS100 in Normal Mice

Organ	Time after injection (min)					
	1	5	20	60	120	240
Blood	18.4 ± 2.38	1.54 ± 0.31	0.98 ± 0.09	1.01 ± 0.22	0.74 ± 0.15	0.66 ± 0.06
Intestine	0.29 ± 0.06	0.19 ± 0.03	0.23 ± 0.08	0.26 ± 0.05	0.23 ± 0.07	0.42 ± 0.01
Kidney	2.33 ± 0.32	2.84 ± 0.36	3.33 ± 0.49	3.24 ± 0.59	3.49 ± 0.28	4.00 ± 0.29
Liver	34.9 ± 2.60	58.9 ± 6.50	62.6 ± 8.10	62.1 ± 4.16	57.8 ± 8.75	59.3 ± 3.03
Stomach	0.27 ± 0.08	0.53 ± 0.28	0.21 ± 0.06	0.29 ± 0.10	0.31 ± 0.15	0.41 ± 0.17
Spleen	14.3 ± 4.42	42.4 ± 11.4	36.7 ± 7.40	40.9 ± 7.32	42.3 ± 10.9	44.5 ± 4.71
Pancreas	0.50 ± 0.07	0.36 ± 0.01	0.30 ± 0.06	0.48 ± 0.27	0.30 ± 0.06	0.30 ± 0.07
Lung	9.51 ± 3.81	1.49 ± 0.16	0.99 ± 0.10	1.17 ± 0.57	0.72 ± 0.08	0.76 ± 0.12
Heart	2.50 ± 0.64	0.61 ± 0.13	0.46 ± 0.06	0.49 ± 0.09	0.42 ± 0.07	0.44 ± 0.04

Each value represents mean ± SD (percentage injected dose per gram of tissue, $n = 4$ or 5).

($n = 4$ for each time-pint). At the designated time intervals, the mice were sacrificed and their organs were dissected. Tissues were weighed, and radioactivity was measured by automated γ counting. Data were calculated as the percentage injected dose per gram of tissue. The blood curves were fitted with PMOD software (PMOD Technologies Ltd.), and the half-lives were determined.

Ex Vivo Autoradiography in apoE−/− Mice

Twenty-four apoE−/− mice (27 wk old, $n = 6$) were used for ex vivo autoradiography studies. Five-week-old ApoE–/– mice were fed a high-fat diet (Clinton/Cybulsky Rodent Diet D12108 with 1.25% cholesterol; Research Diets) for 22 wk. The mice received injections of ^{111}In-PS100, ^{111}In-PC100, ^{111}In-PS200, or ^{111}In-PC200 (5.6 MBq, 100 μL) via the tail vain. Two hours after injection, the mice were euthanized by an overdose of sodium pentobarbital by injection, and the aortic arch and aorta were fixed by cardiac perfusion with 10% neutral-buffered formalin. Dissected arteries were opened longitudinally and exposed on a phosphor imaging plate (Fuji Imaging Plate BAS-UR; Fujifilm Corp.) for 19 h. Autoradiographic images were obtained and analyzed by a computerized imaging analysis system (Bio-Imaging Analyzer FLA 3000; Fujifilm Corp.). Additionally, aortic tissues were stained with oil red O for plaque area determination. Five regions of interest were placed on the plaque area (target) and the nonplaque area (nontarget) in the aortic tissue, and 3 ROIs were placed for background area around each aorta in autoradiography images. Signal intensities were shown as photostimulated luminescence per unit area (PSL/mm^2), and average values for each were used for the analysis. The target-to-nontarget ratios (TNRs) were calculated as follows

$$\text{TNR} = (\text{[target signal]} - \text{[background signal]})/(\text{[nontarget signal]} - \text{[background signal]}).$$

The timeline diagram is given in Figure 1A.

SPECT/CT Imaging with WHHL Rabbits

WHHL rabbits ($n = 2$ per group for ^{111}In-PS100 and ^{111}In-PS200; age, 17 mo; weight, 3.3–3.5 kg) or control New Zealand White rabbits ($n = 2$ for ^{111}In-PS200; age, 17 mo; weight, 3.4 kg) were used for SPECT imaging studies. The animals were anesthetized, and ^{111}In-PS100 or ^{111}In-PS200 (74 MBq) was injected into a marginal ear vein. SPECT scanning was performed 48 h after injection of liposomes using an FX system PET/SPECT/CT scanner (Gamma-Medica Inc.). After the SPECT study, a CT angiogram was acquired. The details are described in the Supplemental Appendix.

After the last scan, rabbits were sacrificed by an overdose of sodium pentobarbital. The aorta was removed, and 10- and 5-μm-thick consecutive sections were prepared. The autoradiogram was obtained with a phosphor imaging system (FLA-3000; Fujifilm Corp.) with 10-μm-thick sections. Other 5-μm-thick sections were subjected to immunohistochemical staining for macrophages, Azan-Mallory staining, and oil red O staining. Immunohistochemistry was performed according to the method reported by Tsukada et al. using the rabbit

TABLE 2
Biodistribution of ^{111}In-PS200 in Normal Mice

Organ	Time after injection (min)					
	1	5	20	60	120	240
Blood	13.1 ± 5.88	3.16 ± 0.55	3.29 ± 0.57	2.92 ± 0.36	2.44 ± 0.50	1.95 ± 0.53
Intestine	0.48 ± 0.12	0.46 ± 0.08	0.44 ± 0.09	0.61 ± 0.16	0.68 ± 0.24	0.86 ± 0.26
Kidney	3.89 ± 1.05	8.98 ± 1.53	9.23 ± 1.96	8.95 ± 1.31	11.0 ± 3.48	12.0 ± 3.07
Liver	22.3 ± 5.96	32.8 ± 5.01	35.2 ± 3.47	36.0 ± 3.30	37.1 ± 6.12	39.1 ± 2.00
Stomach	0.41 ± 0.14	0.38 ± 0.11	0.45 ± 0.06	0.46 ± 0.13	0.39 ± 0.09	0.57 ± 0.22
Spleen	6.05 ± 2.09	20.7 ± 5.73	17.8 ± 5.38	19.0 ± 5.89	21.2 ± 2.96	23.8 ± 5.35
Pancreas	1.05 ± 0.10	0.83 ± 0.14	0.70 ± 0.08	0.83 ± 0.04	0.66 ± 0.11	0.76 ± 0.09
Lung	9.93 ± 2.53	2.59 ± 0.47	2.37 ± 0.35	2.22 ± 0.39	2.14 ± 0.49	1.60 ± 0.36
Heart	2.44 ± 0.79	1.09 ± 0.17	1.01 ± 0.16	1.11 ± 0.22	0.93 ± 0.15	0.91 ± 0.25

Each value represents mean ± SD (percentage injected dose per gram of tissue, $n = 4$ or 5).

TABLE 3
Biodistribution of ^{111}In-PC100 in Normal Mice

Organ	Time after injection (min)					
	1	5	20	60	120	240
Blood	32.9 ± 4.08	30.1 ± 0.46	17.0 ± 5.99	5.75 ± 4.63	0.52 ± 0.49	1.58 ± 1.96
Intestine	0.40 ± 0.05	0.46 ± 0.06	0.37 ± 0.16	0.28 ± 0.13	0.23 ± 0.10	0.59 ± 0.33
Kidney	3.43 ± 0.50	3.51 ± 0.17	3.02 ± 0.96	2.28 ± 0.99	1.56 ± 0.38	3.39 ± 1.63
Liver	6.34 ± 1.67	12.5 ± 2.66	28.1 ± 6.65	47.2 ± 5.75	53.8 ± 6.85	46.5 ± 13.4
Stomach	0.45 ± 0.14	0.56 ± 0.23	0.43 ± 0.14	0.40 ± 0.16	0.39 ± 0.21	0.44 ± 0.14
Spleen	5.16 ± 2.77	17.9 ± 3.20	101 ± 32.6	171 ± 69.4	174 ± 68.3	193 ± 53.7
Pancreas	0.65 ± 0.14	0.66 ± 0.09	0.54 ± 0.25	0.32 ± 0.21	0.21 ± 0.19	0.84 ± 0.48
Lung	18.9 ± 7.76	11.8 ± 1.51	6.62 ± 1.91	3.48 ± 2.55	0.64 ± 0.50	2.66 ± 2.20
Heart	4.33 ± 0.88	3.31 ± 1.00	2.08 ± 0.76	0.78 ± 0.63	0.19 ± 0.07	0.53 ± 0.54

Each value represents mean ± SD (percentage injected dose per gram of tissue, $n = 4$ or 5).

macrophage-specific monoclonal antibody RAM-11 (Dako Corp.) (*26*), and the slices were costained with hematoxylin for identification of the nucleus. The timeline of the experiment is shown in Figure 1B.

Statistical Analysis

Data are presented as the mean ± SD. Statistical analysis was performed using the Mann–Whitney *U* test or paired *t* test for comparisons between or within groups, respectively. Statistical significance was established at a P value of less than 0.05.

RESULTS

In Vitro Uptake of ^{111}In Liposomes by Macrophages

The in vitro uptake of ^{111}In-labeled liposomes and ^{111}In-$InCl_3$ by mouse peritoneal macrophages is summarized in Figure 2. Uptake of both sizes of liposomes was significantly higher for PS than for PC liposomes. ^{111}In-PS100 showed significantly higher uptake than ^{111}In-PS200. D-serine liposomes accumulated in macrophages, but the level was lower than for L-serine liposomes of each size. Only a slight uptake of ^{111}In-$InCl_3$ was observed.

Biodistribution Studies in Normal Mice

Biodistribution data are summarized in Tables 1–4. High liver uptake was observed for all liposomes investigated. Uptake into the spleen was higher for PC liposomes than PS liposomes. Blood clearance was faster for PS liposomes than PC liposomes, and ^{111}In-PC100 showed the slowest clearance. The blood half-lives were 3.2, 22.0, 3.6, and 7.4 min for ^{111}In-PS100, ^{111}In-PC100, ^{111}In-PS200, and ^{111}In-PC200, respectively.

Ex vivo Autoradiography in apoE−/− Mice

En face ex vivo autoradiography showed accumulation of all investigated ^{111}In liposomes in the plaque area in mice (Figs. 3A–3C). Radioactive regions were well matched with oil red O staining. The uptake to nonspecific regions was higher in PC liposomes, and the TNRs were lower in PC liposomes than PS liposomes (Fig. 3D). The TNRs were 2.62 ± 0.16, 2.23 ± 0.13, 3.27 ± 0.49, and 2.51 ± 0.34 for ^{111}In-PS100, ^{111}In-PC100, ^{111}In-PS200, and ^{111}In-PC200, respectively.

SPECT Imaging, Ex Vivo Autoradiography, and Histologic Analysis in WHHL Rabbits

Figure 4 summarizes the SPECT, autoradiography, and histologic images in WHHL and normal rabbits. The arrows indicate the position of the aorta. The atherosclerotic regions were successfully visualized with ^{111}In-PS200 and ^{111}In-PS100, and the clearest image was obtained with ^{111}In-PS200. No aortic accumulation was seen in normal rabbits with ^{111}In-PS200. Autoradiography images of the aortic section showed accumulation of radioactivity in the plaque area in WHHL rabbits. High accumulation of radioactivity was observed in the macrophage foam cell area, and radioactivity was low in the fibrotic area as shown by Azan-Mallory staining.

TABLE 4
Biodistribution of ^{111}In-PC200 in Normal Mice

Organ	Time after injection (min)					
	1	5	20	60	120	240
Blood	33.2 ± 4.03	18.6 ± 5.01	6.83 ± 3.47	2.57 ± 1.33	1.10 ± 0.13	0.65 ± 0.10
Intestine	0.36 ± 0.07	0.31 ± 0.05	0.27 ± 0.03	0.28 ± 0.07	0.32 ± 0.14	0.32 ± 0.09
Kidney	3.35 ± 0.62	3.38 ± 0.51	4.81 ± 1.03	4.38 ± 0.75	4.72 ± 0.67	5.41 ± 1.02
Liver	8.08 ± 2.32	26.7 ± 8.32	38.6 ± 4.17	48.8 ± 3.38	49.4 ± 6.14	46.2 ± 7.84
Stomach	0.54 ± 0.22	0.44 ± 0.16	0.44 ± 0.13	0.40 ± 0.14	0.33 ± 0.20	0.28 ± 0.11
Spleen	10.0 ± 4.24	49.4 ± 12.2	72.2 ± 15.5	112 ± 30.3	142 ± 43.8	173 ± 76.2
Pancreas	0.71 ± 0.27	0.58 ± 0.18	0.44 ± 0.14	0.43 ± 0.10	0.45 ± 0.15	0.38 ± 0.15
Lung	20.8 ± 3.74	9.89 ± 1.79	4.20 ± 1.95	2.00 ± 0.74	1.62 ± 1.02	0.99 ± 0.24
Heart	6.05 ± 2.53	2.95 ± 1.71	1.02 ± 0.39	0.56 ± 0.22	0.49 ± 0.13	0.33 ± 0.07

Each value represents mean ± SD (percentage injected dose per gram of tissue, $n = 4$ or 5).

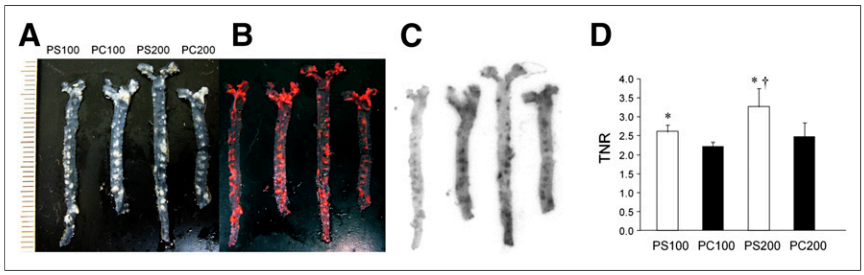

FIGURE 3. En face autoradiography of apoE−/− mice aorta. Photographic images of unstained aorta (A), images after oil red O staining (B), autoradiograms (C), and TNR (D). Autoradiography results were consistent with results of oil red O staining. TNR was significantly higher in PS liposomes than PC liposomes for all liposome sizes (*$P < 0.05$). TNR was higher for PS200 than PS100 (†$P < 0.05$).

DISCUSSION

Macrophage infiltration plays a pivotal role in plaque rupture by releasing inflammatory cytokines and proteases; therefore, it is reasonable to target macrophages for vulnerable plaque imaging. Also, it is well known that macrophages are predisposed to phagocytize particles such as liposomes (*16,17*), and several liposome-based imaging probes have been reported recently (*27,28*). Therefore, in this study, we used liposomes as carriers for the atherosclerotic region and designed a SPECT imaging probe. In fact, cultured macrophages took up control PC liposomes to a certain extent (Fig. 2). Uptake was higher with 100- versus 200-nm liposomes. In addition, when the eat-me signal, PS, was incorporated into the liposome, uptake into cultured macrophages was significantly elevated; furthermore, the uptake of D-PS into macrophages was lower than that of the naturally occurring L isoform of PS (Fig. 2). These results suggest that macrophage targeting using liposomes was successful and that target specificity was enhanced by PS modification. D-PS liposomes showed higher accumulation in macrophages than in PC liposomes for each liposome size. The negative charge on the surface of the liposome may enhance particle capture by macrophages. We previously reported that ^{18}F-FDG uptake into cultured mouse peritoneal macrophages was 48.8 percentage dose per milligram of protein (%dose/mg protein) with a 3-h incubation (*29*). In this study, the uptake of ^{111}In-PS100 (60.5 % dose/mg protein) was greater than that of ^{18}F-FDG. These results show the potential of ^{111}In-PS100 for in vivo atherosclerotic plaque imaging.

The atherosclerotic regions were successfully visualized with ^{111}In-labeled PS liposomes in apoE−/− mice with en face autoradiography after the intravenous injection of the tracers. In contrast with the in vitro results, accumulation was higher for ^{111}In-PS200 than ^{111}In-PS100. Atherosclerotic lesions were visualized by ^{111}In-labeled PC liposomes of both sizes, but nonspecific accumulation was higher with PC liposomes than PS liposomes; thus, TNRs were higher for PS liposomes than PC liposomes. The highest TNR was obtained with ^{111}In-PS200 in the en face autoradiography in apoE−/− mice. Also, successful SPECT imaging was possible with ^{111}In-PS200 in WHHL rabbits. Thus, ^{111}In-PS200 showed the best features for in vivo imaging, although ^{111}In-PS100 provided the best results in in vitro investigations.

In the biodistribution study in normal mice, ^{111}In-PS200 showed somewhat slower blood clearance than ^{111}In-PS100. This difference may result in higher accumulation of ^{111}In-PS200 than ^{111}In-PS100 in atherosclerotic regions of apoE−/− mice, although the uptake was higher in ^{111}In-PS100 in in vitro experiments. Also, we observed a slower blood clearance of PC liposomes than PS liposomes. These results suggest that slow blood clearance should accelerate liposome accumulation into the plaque. However, in atherosclerosis imaging, signals from the blood pool disturb the visualization of plaque in the vessel wall; thus, blood clearance of the imaging probe should ideally be not too slow, and excessive liver uptake makes it difficult to visualize the small atherosclerotic region in coronary arteries. In general, PEGylation of particles prolongs the blood clearance because of the avoidance from the reticuloendothelial system, and liver accumulation would be decreased by PEGylation (*30*). However, because the high liver accumulation can be explained by the liposome uptake into the Kupffer cells, which have characteristics similar

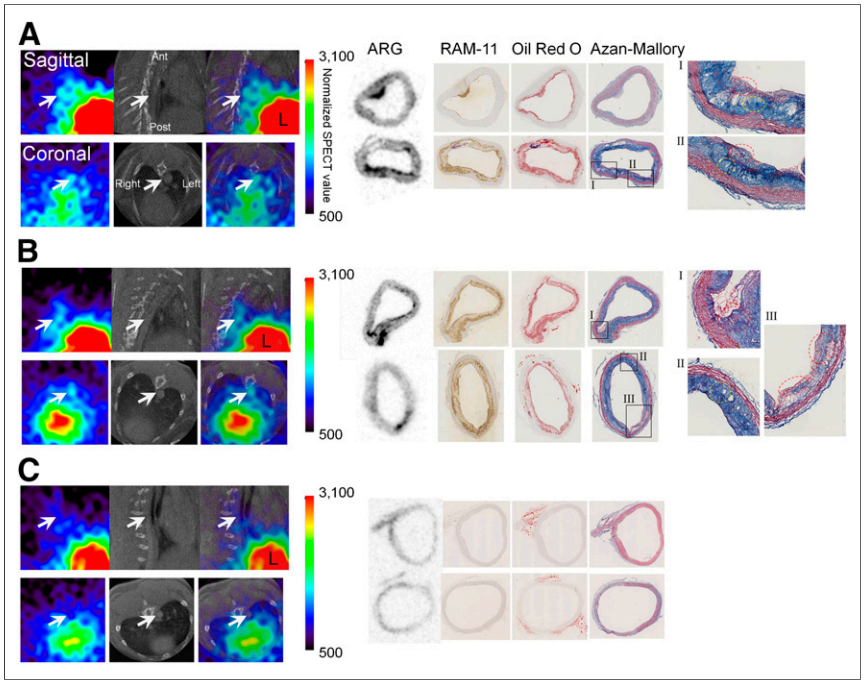

FIGURE 4. SPECT and CT images, ex vivo autoradiography, and histologic images of ^{111}In-PS100 (A) and ^{111}In-PS200 (B) in WHHL rabbits and ^{111}In-PS200 in normal rabbit (C). Arrows indicate position of aorta. L represents liver. Magnified images of Azan-Mallory staining show macrophage foam cell–rich region with less smooth muscle cells (dashed red circle) and a more fibrotic region with dead macrophages (dashed yellow circle). Atherosclerotic regions were successfully visualized with ^{111}In-PS200 and ^{111}In-PS100 in WHHL rabbits. Radioactivity was accumulated in macrophage foam cell area and was low in fibrotic area. No aortic accumulation was seen in normal rabbit.

to macrophages concerning phagocytosis, the too-low accumulation to the liver would cause the decreased uptake to the macrophages in atherosclerotic lesions. Therefore, for atherosclerosis imaging, a certain level of PEGylation of liposomes is desirable, which prolongs blood clearance to a limited extent and which does not disturb phagocytosis by macrophages. Further investigation of liposome PEGylation would be required, to determine the optimal balance between macrophage-targeting ability and desirable blood clearance. In addition, the prolonged retention to the liver might have come from the transchelation of ^{111}In with transferrin (*31,32*). Radiolabeling with ^{99m}Tc might improve the kinetics and reduce the radiation dose. Liposomes can act as a platform for various other imaging modalities, such as MR imaging and optical imaging. Recently, several liposome-based atherosclerosis imaging probes for various imaging modalities have been reported (*33–35*). Because liposomes are biocompatible and have long histories as drug carriers for human use (*36*), such imaging probes, including the liposome system we have described, should be good candidates for clinical use in the future.

CONCLUSION

In this study, the atherosclerotic region was detectable by macrophage targeting with radiolabeled liposomes (PS liposomes), although additional investigations would be needed to improve the in vivo biodistribution and plaque accumulation level.

DISCLOSURE

The costs of publication of this article were defrayed in part by the payment of page charges. Therefore, and solely to indicate this fact, this article is hereby marked "advertisement" in accordance with 18 USC section 1734. This work was supported by grants-in-aid for scientific research from the Japan Science and Technology Agency (JST), Japan Society for the Promotion of Science (JSPS), and Japanese Ministry of Health, Labour and Welfare. No other potential conflict of interest relevant to this article was reported.

REFERENCES

1. Libby P. What have we learned about the biology of atherosclerosis? The role of inflammation. *Am J Cardiol.* 2001;88(7B):3J–6J.
2. Libby P. Inflammation in atherosclerosis. *Nature.* 2002;420:868–874.
3. Rudd JH, Warburton EA, Fryer TD, et al. Imaging atherosclerotic plaque inflammation with [^{18}F]-fluorodeoxyglucose positron emission tomography. *Circulation.* 2002;105:2708–2711.
4. Ogawa M, Ishino S, Mukai T, et al. ^{18}F-FDG accumulation in atherosclerotic plaques: immunohistochemical and PET imaging study. *J Nucl Med.* 2004; 45:1245–1250.
5. Zhang Z, Machac J, Helft G, et al. Non-invasive imaging of atherosclerotic plaque macrophage in a rabbit model with F-18 FDG PET: a histopathological correlation. *BMC Nucl Med.* 2006;6:3.
6. Fifer KM, Qadir S, Subramanian S, et al. Positron emission tomography measurement of periodontal ^{18}F-fluorodeoxyglucose uptake is associated with histologically determined carotid plaque inflammation. *J Am Coll Cardiol.* 2011; 57:971–976.
7. Tawakol A, Migrino RQ, Bashian GG, et al. In vivo ^{18}F-fluorodeoxyglucose positron emission tomography imaging provides a noninvasive measure of carotid plaque inflammation in patients. *J Am Coll Cardiol.* 2006;48:1818–1824.
8. Rudd JH, Myers KS, Bansilal S, et al. Atherosclerosis inflammation imaging with ^{18}F-FDG PET: carotid, iliac, and femoral uptake reproducibility, quantification methods, and recommendations. *J Nucl Med.* 2008;49:871–878.
9. Rudd JH, Myers KS, Bansilal S, et al. Relationships among regional arterial inflammation, calcification, risk factors, and biomarkers: a prospective fluorodeoxyglucose positron-emission tomography/computed tomography imaging study. *Circ Cardiovasc Imaging.* 2009;2:107–115.
10. Chen W, Bural GG, Torigian DA, Rader DJ, Alavi A. Emerging role of FDG-PET/CT in assessing atherosclerosis in large arteries. *Eur J Nucl Med Mol Imaging.* 2009;36:144–151.
11. Deichen JT, Prante O, Gack M, Schmiedehausen K, Kuwert T. Uptake of [^{18}F] fluorodeoxyglucose in human monocyte-macrophages in vitro. *Eur J Nucl Med Mol Imaging.* 2003;30:267–273.
12. Bucerius J, Mani V, Moncrieff C, et al. Impact of noninsulin-dependent type 2 diabetes on carotid wall ^{18}F-fluorodeoxyglucose positron emission tomography uptake. *J Am Coll Cardiol.* 2012;59:2080–2088.
13. Medina OP, Zhu Y, Kairemo K. Targeted liposomal drug delivery in cancer. *Curr Pharm Des.* 2004;10:2981–2989.
14. Koo OM, Rubinstein I, Onyuksel H. Role of nanotechnology in targeted drug delivery and imaging: a concise review. *Nanomedicine.* 2005;1:193–212.
15. Lim SB, Banerjee A, Onyuksel H. Improvement of drug safety by the use of lipid-based nanocarriers. *J Control Release.* 2012;163:34–45.
16. Stossel TP. Phagocytosis (first of three parts). *N Engl J Med.* 1974;290:717–723.
17. Pratten MK, Lloyd JB. Pinocytosis and phagocytosis: the effect of size of a particulate substrate on its mode of capture by rat peritoneal macrophages cultured in vitro. *Biochim Biophys Acta.* 1986;881:307–313.
18. Fadok VA, Voelker DR, Campbell PA, Cohen JJ, Bratton DL, Henson PM. Exposure of phosphatidylserine on the surface of apoptotic lymphocytes triggers specific recognition and removal by macrophages. *J Immunol.* 1992;148:2207–2216.
19. Tait JF, Smith C. Phosphatidylserine receptors: role of CD36 in binding of anionic phospholipid vesicles to monocytic cells. *J Biol Chem.* 1999;274: 3048–3054.
20. Henson PM, Bratton DL, Fadok VA. Apoptotic cell removal. *Curr Biol.* 2001;11: R795–R805.
21. Oussoren C, Storm G. Liposomes to target the lymphatics by subcutaneous administration. *Adv Drug Deliv Rev.* 2001;50:143–156.
22. Lindh I, Stawinski J. A general method for the synthesis of glycerophospholipids and their analogs via H-phosphonate intermediates. *J Org Chem.* 1989;54:1338–1342.
23. Ogihara-Umeda I, Sasaki T, Kojima S, Nishigori H. Optimal radiolabeled liposomes for tumor imaging. *J Nucl Med.* 1996;37:326–332.
24. Mauldin JP, Srinivasan S, Mulya A, et al. Reduction in ABCG1 in Type 2 diabetic mice increases macrophage foam cell formation. *J Biol Chem.* 2006;281:21216–21224.
25. Lowry OH, Rosebrough NJ, Farr AL, Randall RJ. Protein measurement with the Folin phenol reagent. *J Biol Chem.* 1951;193:265–275.
26. Tsukada T, Rosenfeld M, Ross R, Gown AM. Immunocytochemical analysis of cellular components in atherosclerotic lesions: use of monoclonal antibodies with the Watanabe and fat-fed rabbit. *Arteriosclerosis.* 1986;6:601–613.
27. Almer G, Frascione D, Pali-Scholl I, et al. Interleukin-10: an anti-inflammatory marker to target atherosclerotic lesions via PEGylated liposomes. *Mol Pharm.* 2013;10:175–186.
28. Bhavane R, Badea C, Ghaghada KB, et al. Dual-energy computed tomography imaging of atherosclerotic plaques in a mouse model using a liposomal-iodine nanoparticle contrast agent. *Circ Cardiovasc Imaging.* 2013;6:285–294.
29. Ogawa M, Nakamura S, Saito Y, Kosugi M, Magata Y. What can be seen by ^{18}F-FDG PET in atherosclerosis imaging? The effect of foam cell formation on ^{18}F-FDG uptake to macrophages in vitro. *J Nucl Med.* 2012;53:55–58.
30. Milla P, Dosio F, Cattel L. PEGylation of proteins and liposomes: a powerful and flexible strategy to improve the drug delivery. *Curr Drug Metab.* 2012;13: 105–119.
31. Kimura Y, Fujii T, Ochi K, Akamune A, Hamamoto K. In vitro and in vivo effects of diethylene triamine penta-acetic acid on the distribution of indium-111 monoclonal antibody metabolism. *Eur J Nucl Med.* 1992;19:759–764.
32. Reilly R, Lee N, Houle S, Law J, Marks A. In vitro stability of EDTA and DTPA immunoconjugates of monoclonal antibody 2G3 labeled with indium-111. *Int J Rad Appl Instrum [A].* 1992;43:961–967.
33. Mulder WJ, Douma K, Koning GA, et al. Liposome-enhanced MRI of neointimal lesions in the ApoE-KO mouse. *Magn Reson Med.* 2006;55:1170–1174.
34. Li D, Patel AR, Klibanov AL, et al. Molecular imaging of atherosclerotic plaques targeted to oxidized LDL receptor LOX-1 by SPECT/CT and magnetic resonance. *Circ Cardiovasc Imaging.* 2010;3:464–472.
35. Almer G, Wernig K, Saba-Lepek M, et al. Adiponectin-coated nanoparticles for enhanced imaging of atherosclerotic plaques. *Int J Nanomedicine.* 2011;6: 1279–1290.
36. Torchilin VP. Recent advances with liposomes as pharmaceutical carriers. *Nat Rev Drug Discov.* 2005;4:145–160.